Electrooxidation of Carbon Monoxide on Gold Nanoparticle Ensemble Electrodes: Effects of Particle Coverage

Sachin Kumar and Shouzhong Zou*

Department of Chemistry and Biochemistry, Center for Nanotechnology, Miami University, Oxford, Ohio 45056

Received: April 16, 2005; In Final Form: May 30, 2005

Gold nanoparticles were attached to amine-functionalized indium tin oxide substrate to form particle ensemble electrodes with controlled particle coverage. Electrooxidation of carbon monoxide (CO) on these particle ensemble electrodes was studied in CO-saturated alkaline solutions by means of cyclic voltammetry, with an emphasis on the effects of particle coverage. CO oxidation half-wave potential was found to decrease with increasing particle density. However, the current density was significantly larger at lower particle coverage electrodes. On the basis of a model for electron transfer on a partially covered electrode, the observations were explained in terms of the change in reactant mass transport pattern with varying particle coverages: CO diffusion is predominantly mixed spherical and linear at low particle coverages and changes to mostly linear at high particle coverages. The possibility of contributions from particle agglomeration is also briefly discussed.

I. Introduction

A central issue in heterogeneous catalysis is to explore the relationship between catalytic activity/selectivity and catalyst surface structure. An extensively used approach utilizes single-crystal surfaces to model catalyst surfaces, taking advantage of their regular and reproducible structures.[1−3] By use of this approach, significant advancement in our understanding of catalytic reactions at both solid−gas and solid−liquid interfaces has been achieved.[1−5] However, a limitation of using single crystal surfaces is whether the results from the well-defined surfaces are representative to the catalysts used in practice, which are typically nanoparticles. Recent experimental results reveal that nanoparticles can have drastically different reactivity from their bulk. For example, small gold nanoparticles supported on oxide surfaces show a high activity toward carbon monoxide (CO) oxidation in the gas phase, but bulk gold surface is largely inert to the reaction.[6,7] For electrochemical reactions, reduction of O_2 was found to proceed via four-electron route on Au nanoparticles, while two-electron reduction is predominant on bulk Au electrodes.[8,9] It is therefore of both fundamental and practical importance to study the reactivity of nanoparticles and bridge the knowledge gap between single-crystal surfaces and particle surfaces.

The idea of studying particle reactivity is not new in surface science. The limitation of such a practice in the past was the lack of control in the particle structure. Recent rapid advancement of nanoparticle synthesis/fabrication catalyzed by current interests in nanoscience and technology provides a means to reveal the relationship between particle structure (including size, shape, and interparticle distance) and reactivity in an unprecedented controlled fashion. Nanoparticles with monodispersity and sometimes even with a regular shape have been made, and new surface chemistry is evolving.[10−13] In solution reactions, El-Sayed's group studied in a great detail the Suzuki reaction catalyzed by Pd nanoparticles and the electron-transfer reaction between $Fe(CN)_6^{3-}$ and thiosulfate.[14−16] In gas-phase environment, Somorjai and co-workers studied CO oxidation on uniform Pt nanoparticle arrays supported on alumina made by electron beam lithography and found that the activation energy on the nanoparticle array is much smaller than that on Pt(111) surface.[17] For electrochemical reactions, O_2 reduction and CO oxidation have been studied on Au or Pt nanoparticles. El-Deab and Ohsaka showed that four-electron O_2 reduction was catalyzed by Au nanoparticles electrodeposited on Au electrodes.[8,9] Dong and co-workers studied O_2 reduction on Pt thin film coated Au nanoparticles.[18] *Solution* CO and methanol electrooxidation on monolayer-protected Au nanoparticles in alkaline solutions has been studied by Zhong's group.[19−21] Recently McFarland and co-worker investigated *solution* CO electrooxidation on Au nanoparticles uniformly assembled on indium tin oxide (ITO) coated glass slides.[22,23] Friedrich et al. and Savinova et al. studied the CO *monolayer* oxidation on different-sized Pt nanoparticles supported on Au or glassy carbon electrodes and found that CO oxidation occurs at higher overpotentials on smaller particles.[24−27] A particle coverage dependence of *adsorbed* CO oxidation peak potential was also demonstrated.[24,27]

Herein we report the electrooxidation of *solution* CO in basic solutions on Au nanoparticle ensemble electrodes containing various amounts of particles, with a focus on the effects of particle coverage. A unique feature of this system is that only the Au nanoparticles are active for CO oxidation; the particle-free regions are inactive. Therefore, it allows studying the reaction on Au nanoparticles without the need to block the ITO surfaces, as long as the capacitive charging current is small as compared to the Faradaic current. These nanoparticle ensemble electrodes are then practically nanoparticle array electrodes or partially blocked electrodes with nanometer-sized active sites.[28−33]

Cyclic voltammetric results show that, with increasing particle coverage, the half-wave potential for CO oxidation decreases. However, the oxidation current density was significantly larger on the lower particle density ensemble electrodes, regardless of particle size. By use of a model for electron transfer at a partially blocked electrode, the observations can be understood in terms of the CO diffusion pattern change.[29] At low particle

* To whom all correspondence should be addressed. Tel: 513-529 8084. Fax: 513-529 5715. E-mail: zous@muohio.edu.

10.1021/jp051981a CCC: $30.25
Published on Web 07/29/2005

coverages, a mixed spherical and linear diffusion is dominant, while at high particle coverages, a semi-infinite linear diffusion is predominant. The study shows that the shift of reaction potential alone in a voltammogram does not necessarily mean the reactivity change. When comparing results from particle electrodes, it is important to know the particle coverage, especially at low particle coverages. Given the increasing interests in studying particle structure−reactivity relationship in electrocatalysis, the present findings are of both fundamental and practical importance.

II. Experimental Section

Chemicals. Hydrogen tetrachloroaurate trihydrate ($HAuCl_4 \cdot 3H_2O$), sodium borohydride ($NaBH_4$), (3-amino-propyl)trimethoxysilane (APTMS), and trisodium citrate were obtained from Sigma-Aldrich, and ethanolamine was obtained from Alfa Aeser. Semiconductor grade (99.997%) carbon monoxide was from Spectra Gas (Branchburg, NJ). All the chemicals were used as received, and all the aqueous solutions were prepared using Milli-Q water from a Millipore water purification system (Milli-Q A10, Millipore, MA).

Instruments. UV−vis absorption spectra of Au colloidal solutions were measured with an Agilent 8453 spectrometer. Atomic force microscopy (AFM) images of Au nanoparticles assembled on ITO-coated glass slides (resistance 4−6 Ω·cm, Delta Technologies, MN) were obtained using a PicoPlus II scanning probe microscope (Molecular Imaging, AZ). Cyclic voltammograms were recorded in a conventional two-compartment three-electrode cell using an electrochemical analyzer (CHI 630, CH Instruments, TX). A Pt wire served as the counter-electrode, and a Ag/AgCl (with saturated KCl) was used as the reference electrode. The cell resistance was compensated with the *iR* compensation function in the analyzer software. All the measurements were done at room temperature (23 ± 1 °C).

Preparation of Au Particles. All glassware used for colloid preparations were thoroughly cleaned in aqua regia (3:1 v/v concentrated HCl and HNO_3), rinsed with Milli-Q water, and soaked in water for 1 h prior to use. The 3-nm Au particles were prepared according to the method reported by Natan's group.[34] Briefly, 1 mL of 1% $HAuCl_4$ was diluted in 90 mL of water at room temperature and stirred for 1 min before 2 mL of 38.8 mM sodium citrate were added to this solution. After stirring for another minute, 1 mL of freshly prepared 0.075 wt % solution of $NaBH_4$ in 38.8 mM sodium citrate was added and the solution turned purple immediately. The colloidal solution was stirred for 5 more min and then stored in dark at 4 °C. A UV−vis spectrum of the prepared Au colloid showed a plasmon absorption peak at ca. 510 nm, which agrees with the reported spectrum of 3-nm Au particles. The particle solution is stable against aggregation over a period of at least one month as indicated by the unchanged UV−vis absorption spectrum.

The 12-nm Au particles were synthesized followed the method reported by Grabar et al.[35] Briefly, 100 mL of 1 mM $HAuCl_4$ aqueous solution were heated to boil in a 250-mL round-bottom flask. Sodium citrate (10 mL, 38.8 mM) were added swiftly with stirring. The solution turned clear then blue and finally deep red in 30 s. The solution was kept boiling and stirring for another 15 min before it was cooled and stored in the dark at 4 °C. The 50−60-nm Au particles were made by an iterative hydroxylamine reduction method which uses the 12-nm Au particles as the "seed".[34]

Surface Derivatization of Substrate. ITO glass slides were functionalized with APTMS to introduce amine groups as the anchor points for the Au nanoparticles.[35−37] Immediately before the surface derivatization, ITO glass slides were cleaned by sonication successively in 20% v/v ethanolamine aqueous solution and pure methanol for 30 min, followed by thorough rinsing with methanol. The cleaned slides were then soaked in 40 mM 3-APTMS methanol solution overnight. The derivatized slides were sonicated 1 min followed by thorough rinsing in CH_3OH to remove any loosely attached APTMS molecules.

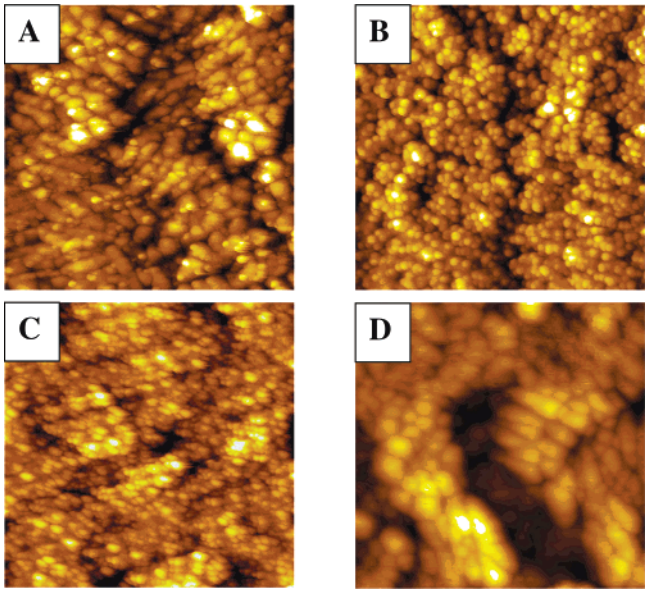

Figure 1. Noncontact mode AFM images obtained from APTMS-derivatized ITO electrodes with various coverages of 3 nm Au particles: (A) 0.01; (B) 0.10; (C) 0.25; (D) no particle. Image size: 500 × 500 nm^2.

Attachment of Au Nanoparticles onto ITO Slides. After the formation of a self-assembled monolayer of APTMS, the ITO slides were dried in an oven at 110 °C for 10 min to remove methanol, followed by immersion in the desired Au colloid solutions for various length of time. The slides were rinsed thoroughly with water after removal from the Au colloid solutions and subsequently dried again at 110 °C for 30 min. The final drying step is important for the AFM characterization.

III. Results and Discussion

1. AFM Images of Gold Nanoparticles Attached to ITO Slides.

As stated in the outset, the main objective of this study is to investigate solution carbon monoxide electrooxidation on Au nanoparticles assembled on ITO slides (hereafter referred to as particle ensemble electrodes), with the emphasis on the influence of particle coverage on the voltammetric behavior. To control the amount of particles on the substrate, a combination of varying soaking time and particle concentration was used. This simple strategy appears to be successful in controlling particle density with acceptable reproducibility. Shown in Figure 1 is a set of AFM images of particle ensemble electrodes with various coverages of 3-nm gold particles. For comparison, an image of an APTMS-coated ITO slide is also presented (Figure 1D). The particle coverage (θ_p) is defined as the ratio between the electrochemically accessible Au nanoparticle area and the geometric area of the ITO slides in contact with the electrolyte solution. The particle area was calculated by using the charge involved in the reduction of the electrochemically formed Au oxide in the cyclic voltammograms recorded between −0.7 and 0.7 V in 0.1 M NaOH (see Supporting Information 1), assuming the charge density for the reduction of the Au oxide is 723 μC/

cm^2 (eq 1).[38] The calculated particle coverage agrees (within 10%) with the value obtained

$$\theta_p = \frac{\text{particle area (cm}^2\text{)}}{\text{ITO geometric area (cm}^2\text{)}} = \frac{\text{Au oxide reduction charge } (\mu\text{C})/723\ (\mu\text{C/cm}^2)}{\text{ITO geometric area (cm}^2\text{)}} \quad (1)$$

by counting the number of particles in the AFM images at low and medium θ_p and assuming the particles have a spherical shape. The particle ensemble shown in Figure 1A was obtained after soaking the APTMS-functionalized ITO slides in a 50% diluted particle solution for 30 s. In the image, gold particles appear as small bright dots with a diameter around 3 nm. The larger dark features are from the ITO slides, as they also appear in an APTMS-modified ITO slide without any Au nanoparticles (see Figure 1D). The particle ensembles obtained in this way typically have a θ_p of 1−2%. Clearly, individual gold nanoparticles are discernible, and they are randomly distributed on the ITO slides with preferential adsorption on the edge of ITO islands. The particle aggregation is negligible, at least in the examined area. By soaking the APTMS-derivatized ITO slides in the as-prepared nanoparticle solution for 10 min, a much higher particle coverage was obtained (Figure 1B). The obtained particle coverage in this case is typically around 10%. Again, the Au particles appear as bright spherical dots and distribute over the entire examined region. Though individual particles are distinguishable, some degree of particle aggregation is apparent. With a further increase in the soaking time to 15 h, many more particles were attached to the substrate (Figure 1C). The particle coverage attainable in this way is around 25−30%. A longer soaking time does not yield a higher particle density, which may result from the repulsive particle−particle interaction due to the negative charges on the particles from the adsorbed citrate layer.[39] The image clearly demonstrates a large degree of particle aggregation; the individual particles are not as distinguishable as those in Figure 1B. These images together with the corresponding cyclic voltammagrams obtained in 0.1 M NaOH (see Supporting Information 1) show that by varying the particle concentration and the soaking time, Au nanoparticle ensemble electrodes with a semicontrollable particle coverage can be obtained.

By use of a similar approach, particle ensemble electrodes made of 12 and 60 nm Au particles were also obtained with a controlled particle coverage. Because the particle concentration in the as-prepared colloidal solution in these two cases is lower, the soaking time required to achieve the same particle coverage was significantly longer, especially for the 60-nm particles. For example, to obtain a 10% coverage of the 60-nm particle, the soaking time was normally around 60 min, as compared to 10 min for the 3-nm particle. The maximum achievable θ_p is also significantly larger than that for the 3-nm particle, about 50% for the 12-nm and 70% for the 60-nm particles. The higher attainable particle density for the larger particles presumably arises from the less compact citrate-protecting layer. This is supported by the observation that the larger particle solutions are less stable as compared to the 3-nm colloidal solution. Particle aggregation was observed within a few days after they were made, especially for the 60-nm particles. The success of obtaining the ensemble electrodes with varying θ_p allows us to examine the influence of the particle coverage on the electrooxidation of CO, which is discussed in the following sections.

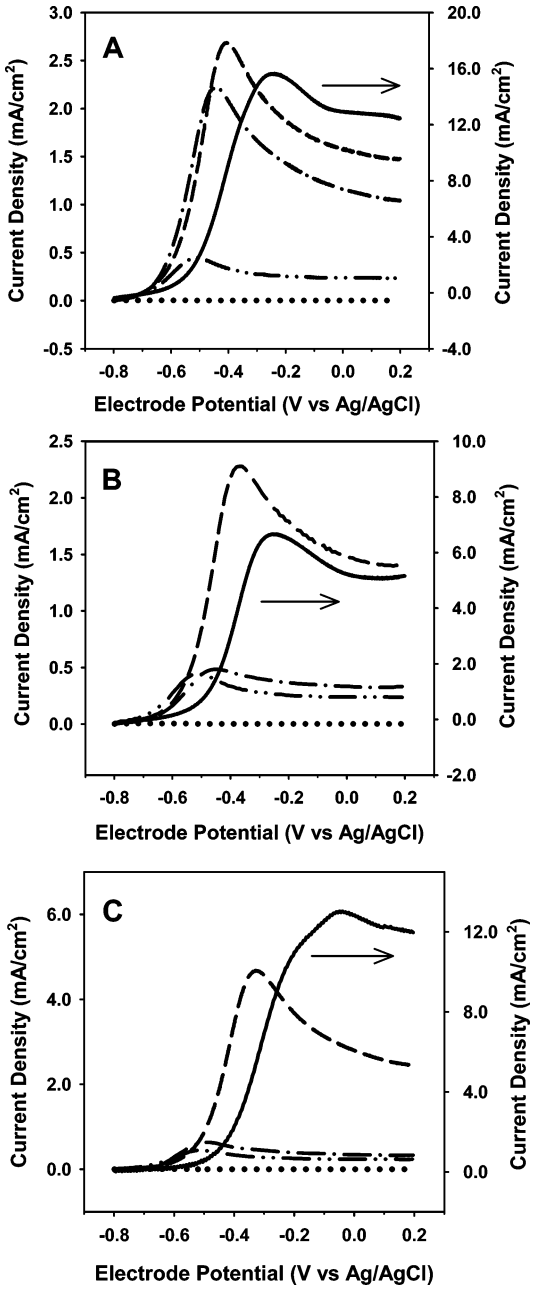

Figure 2. Anodic segments of cyclic voltammograms for CO oxidation obtained in CO saturated 0.1 M NaOH on gold particle ensemble electrodes. (A) 3 nm (θ_p: solid, 0.01; dashed, 0.10; dash−dotted, 0.25); (B) 12 nm (θ_p: solid, 0.03; dashed, 0.15; dash−dotted, 0.50); (C) 60 nm (θ_p: solid, 0.003; dashed, 0.07; dash−dotted, 0.70). In each panel, the dashed−double-dotted trace was from a gold ball electrode and the dotted trace from an APTMS-coated ITO electrode. The solid traces use the *y* axis at the right. Scan rate = 0.1 V s^{-1}.

2. Electrooxidation of Solution Carbon Monoxide

Figure 2 shows anodic segments of cyclic voltammograms of solution CO oxidation on particle ensemble electrodes composed of 3- (A), 12- (B), and 60-nm (C) Au particles, each with three different particle coverages. The CVs were obtained with a 0.1 V s^{-1} scan rate in a *CO-saturated* solution, which was formed by purging CO into the deaerated 0.1 M NaOH solution for 5 min. For clarity, only the first anodic segments were shown. The current decreased in the successive cycles due to the decrease of CO concentration. If the solution was replenished with CO, the current returned to the original value (within 5%). For comparison, the corresponding CV obtained

TABLE 1: Comparison of Electrochemical Kinetic Parameters for CO Electrooxidation at Different Au Electrodes in CO-Saturated 0.1 M NaOH

electrode	θ_p[a]	$E_{p/2}$[b]	$10^3\ k_{app}$[c]	$n\alpha_{app}$[d]
3 nm	0.01	−0.42	0.56	0.42
	0.10	−0.51	2.4	0.43
	0.25	−0.55	4.8	0.48
12 nm	0.03	−0.39	0.34	0.44
	0.15	−0.48	1.33	0.44
	0.50	−0.57	5.7	0.42
60 nm	0.003	−0.32	0.12	0.36
	0.07	−0.43	0.61	0.45
	0.70	−0.60	13.4	0.60
gold ball	N.A.	−0.62	14.5	0.47

[a] Particle coverage calculated as the area ratio between the electrochemically accessible Au area and the ITO glass slide geometric area. [b] Half peak potential (V vs Ag/AgCl) with scan rate = 0.1 V s^{-1}. [c] Apparent rate constant (cm s^{-1}) for CO electro-oxidation at −0.5 V vs Ag/AgCl, extracted from the voltammetric data shown in Figure 2 by using eqs 2 and 3 (see text). [d] Apparent anodic transfer coefficient obtained from the voltammetric data shown in Figure 2 by using eq 3.

from a gold ball electrode formed by melting one end of a Au wire was also included in each panel (dashed−double-dotted traces). The current density was calculated using the electrochemically accessible Au surface area obtained from the Au oxide reduction charge (vide supra). Also contained in Figure 2 is the corresponding CV from APTMS-coated ITO electrodes without Au particles serving as the blank (dotted traces).

The solid trace in Figure 2A was from an ensemble electrode with a $\theta_p \approx 1\%$, the dashed trace with ∼10%, and the dashed−dotted trace with ∼25% of Au nanoparticles. Three interesting trends are apparent in the CVs from the ensemble electrodes. First, the CO oxidation peak potential gradually shifts to more negative values with increasing particle density, e.g., from −0.25 V at $\theta_p = 1\%$ to −0.45 V at $\theta_p = 25\%$, approaching that of the bulk electrode. Second, the current density at low θ_p is considerably larger than that at higher θ_p and on the bulk gold. Third, the shape of the anodic CV changes from pseudosigmoidal at low θ_p to peak at higher θ_p. The anodic CV from the APTMS-coated ITO appears featureless at most potentials except for the region where hydrogen evolution occurs, indicating that CO oxidation does not occur on ITO electrodes without gold particles.

To examine whether the formation of larger particles through particle aggregation is responsible for the more negative CO oxidation peak potential at higher θ_p, we employed ensemble electrodes with 12- and 60-nm Au particles. The cyclic voltammagrams for CO oxidation on these particle ensemble electrodes are displayed in parts B and C of Figure 2 for three different particle coverages. Interestingly, similar trends were also observed. With increasing θ_p, the CO oxidation peak potential shifts to more negative values and the current density decreases significantly, both approaching the corresponding values of the Au ball electrode. As evident in the parts B and C of Figure 2, for the lowest particle coverage, the voltammogram peak is broad and has a pseudosigmoidal shape (this is most noticeable with the 60-nm particles, Figure 2C, solid trace). Similar sigmoidal-shape voltammograms have been observed for As(III) oxidation on Pt nanoparticles at slow scan rates[40] and (trimethylammonia) methyl ferrocene oxidation at pinholes of a thiol monolayer on gold electrodes.[32]

To make a more quantitative comparison, we use the half-wave peak potential ($E_{p/2}$) at which the current is one-half of the peak value. Table 1 summarizes the $E_{p/2}$ for the particle ensemble electrodes examined here, together with the value obtained on the gold ball electrode. The $E_{p/2}$ values evidently decrease with the particle coverage. Close inspection of Table 1 reveals a weak, yet discernible, particle size dependence on the $E_{p/2}$. For example, the $E_{p/2}$ for the 3-nm particle electrode with $\theta_p = 0.01$ is −0.42 V, which is 30 mV more negative than that for the 12-nm particle electrode with $\theta_p = 0.03$.

From the voltammograms, the kinetic data for CO oxidation can be obtained. Following the approach described by Weaver et al.,[41] the apparent (i.e., double layer charging current uncorrected) rate constant (k_{app}, cm s^{-1}) for CO oxidation was evaluated at the peak potential E_p and more negative potentials corresponding to one-half, one-quarter, and one-eighth of the peak current, $E_{p/2}$, $E_{p/4}$, and $E_{p/8}$, respectively, using the following equation

$$\log k_{app} = K + \frac{1}{2}\log(n\alpha_{app}\upsilon DF/RT) \qquad (2)$$

where υ is the scan rate (V s^{-1}), D is the CO diffusion coefficient in aqueous solutions taken as 2×10^{-5} cm^2 s^{-1},[42] F is the Faraday constant (C mol^{-1}), R is the gas constant (J K^{-1} mol^{-1}), T is temperature (K), and n is the number of electrons involved in the reaction. The constant K equals 0.339, −0.469, −0.851, and −1.187 at E_p, $E_{p/2}$, $E_{p/4}$, and $E_{p/8}$, respectively. The apparent transfer coefficient, α_{app}, was obtained from[43]

$$n\alpha_{app} = 47.7\ \text{mV}/(E_p - E_{p/2}) \qquad (3a)$$

$$n\alpha_{app} = 22.5\ \text{mV}/(E_{p/2} - E_{p/4}) \qquad (3b)$$

$$n\alpha_{app} = 20.0\ \text{mV}/(E_{p/4} - E_{p/8}) \qquad (3c)$$

In most cases, the difference of α_{app} values obtained by the above equations is within 10%. In the cases of very small particle coverage, the α_{app} was calculated by the latter two equations because of the large uncertainty in the E_p. The average of α_{app} obtained by using eq 3 was employed in evaluating the k_{app}. The obtained k_{app} and $n\alpha_{app}$ are included in Table 1. For ease of comparison, the k_{app} values are reported at −0.5 V which were obtained by extrapolating/interpolating the $\log(k_{app}) - E$ plot. This potential was chosen to minimize the extrapolation. For the lowest θ_p electrode of the 60-nm particle, the k_{app} at E_p was not included in the $\log(k_{app}) - E$ plot due to the large uncertainty in E_p. Table 1 reveals that at a given potential the higher the particle coverage, the larger the rate constant. At the highest θ_p of the three particles, the k_{app} is very close to that of the gold ball electrode, especially for the 60-nm particle.

Of central interest here is to examine and understand the particle coverage dependence of CO electrooxidation on the nanoparticle ensemble electrodes. The voltammograms clearly demonstrate that the overpotential of CO oxidation decreases with increasing particle coverage, which corresponds to the increase of the reaction rate constant as revealed in Table 1. However, the current density decreases with increasing θ_p, contrary to the Butler−Volmer expression. To understand these observations, it is important to examine the electrode structure. In these particle ensemble electrodes, the active sites for the reaction are the Au nanoparticles; the ITO substrate merely serves as a support and provides the electrical connection (cf. Figure 2). Therefore, the particle ensemble electrodes can be treated as partially blocked electrodes with each of the particles as an active site.

In a model proposed to describe the electron transfer at partially blocked electrodes, Amatore et al. found that, when the blocking coverage (θ) is not close to unity, the observed

current in the CV is the same as if the electrode is not blocked, because of the overlapping of the diffusion field of the neighboring particles.[29] However, the apparent rate constant is lowered by a factor of $(1 - \theta)$. When the blocking coverage is close to unity, the voltammogram is complicated by the mixed linear and spherical reactant diffusion to the electrode. Depending on the reaction rate, blocking coverage, and scan rate, the voltammogram can have the typical diffusion-controlled peak shape or the steady-state sigmoidal polarogram shape. For a slow electron-transfer reaction, the observed rate constant also decreases with increasing blocking coverage. The change of the shape and other characteristics of the voltammogram under different experimental conditions were summarized in the form of a zone diagram in ref 29.

In the present case, the particles on the electrode can be considered as the active sites and the bare ITO as the inactive blocked sites. Therefore the particle coverage (θ_p) is equivalent to the active site coverage $(1 - \theta)$ in ref 29.[44] Since the adsorption of CO on Au is weak, the electrooxidation here can be approximated as a simple electron-transfer reaction. From the zone diagram described in ref 29, the voltammograms of the particle ensemble electrodes should have a diffusion-controlled-type peak shape, except for the $\theta_p = 0.003$ with the 60-nm particle (cf. ref 29). This point lies in the region where the transition from the sigmoidal to peak shape occurs. On the basis of the zone diagram, the peak potential should shift to the negative direction with increasing θ_p. These model predictions agree well with the experimental observations. Thus in the case of $\theta_p = 0.003$ for the 60-nm particle, the largely sigmoidal voltammogram shape reflects the transition from spherical to linear diffusion. For other particle coverages, the voltammograms have a peak shape and the oxidation half-wave potentials shift gradually to more negative values with increasing particle coverage. The corroboration strongly suggests that the apparent increase of CO oxidation activity in the form of a negative shift in $E_{p/2}$ with increasing particle coverage arises from the transition of a mixed spherical and linear diffusion at low particle coverages to a mostly linear diffusion pattern at higher θ_p. The current density for the ensemble electrodes with low particle coverages is much higher than that of the higher coverage electrodes (note the scale difference in Figure 2), indicating a more efficient reactant mass transfer to the electrode in the former case. This strongly supports the above assessment of the diffusion pattern change with the particle coverage.

Another piece of evidence supporting the hypothesis that the change of diffusion pattern is responsible for the increase of apparent activity of CO oxidation can be found from the kinetic analysis of the voltammograms. As revealed in Table 1, the apparent (i.e., double layer uncorrected) rate constant increases with particle coverage. Under the present experimental conditions, the apparent rate constant is expected to be smaller than the standard rate constant (k_0) by a factor of θ_p, based on the model proposed by Amatore et al.[29] Taking the rate constant of CO oxidation on the bulk gold as k_0, the ratio between k_{app} and k_0 should be close to the particle coverage. Figure 3 is a plot of k_{app}/k_0 vs θ_p. The data points include all the electrodes examined in the present work. Although particles with three sizes were used, the difference in k_{app} caused by the particle size is much smaller than that by the particle coverage (vide supra). The plot shows a linear relationship with a slope very close to unity. Given the errors in determining k_{app} and θ_p, the linearity of the plot is reasonably good. This further confirms that the difference of $E_{p/2}$ and hence k_{app} observed on particle ensemble electrodes mainly arises from the diffusion pattern change. An apparent slower electron transfer rate for benzoquinone reduction on gold electrodes partially blocked by a thiol layer has also been observed by Baker and Crooks.[45]

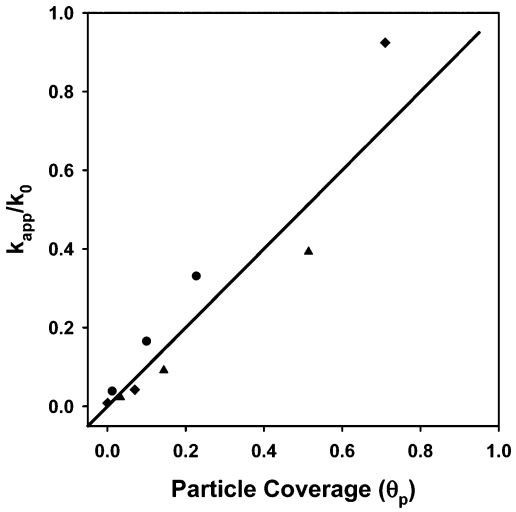

Figure 3. Relative rate constant (k_{app}/k_0) vs particle coverage (θ_p) plot. Data extracted from the voltammograms shown in Figure 2. Symbols: ●, 3-nm particles; ▲, 12-nm particles; ◆, 60-nm particles. The solid line with unity slope serves as a guide to eyes.

Admittedly, a complication of the present study is the increasing degree of particle aggregation with larger θ_p, as evident in the AFM images (Figure 1). The particle aggregation has several effects. First, the aggregation will result in larger particles, which might have a higher activity toward CO oxidation; second, the aggregation may disrupt the citrate layer on the particles, which creates vacant sites for CO oxidation; third, the aggregation forms new structures at the particle−particle junctions which can be more active toward the reaction. We will look at each of these possibilities below.

From Table 1, the $E_{p/2}$ from the smaller particles is typically more negative than the larger ones at a similar θ_p. For example, the $E_{p/2}$ for the 3-nm particles at $\theta_p = 0.01$ is −0.42 V as compared to −0.39 V for the 12-nm particles at $\theta_p = 0.03$. This particle size dependency is in contrast with the hypothesis that the larger particles have a higher activity toward CO electrooxidation. In addition, the $E_{p/2}$ for all the particles examined decreases with increasing particle coverage in a similar fashion. These observations provide solid evidence that the formation of larger particles does not contribute to the observed apparent increasing reactivity. This is in contrast to the *adsorbed* CO oxidation on Pt nanoparticles, at which CO oxidation potential shift to more negative values with larger particles.[24,25,27]

Another possible contribution for the apparent increasing reactivity could be from the loss of the citrate-protecting layer. In the particle synthesis process, citrate was used as both the protecting and reducing agents. No effort was taken to remove the citrate from the particle surface before and after the particle attachment. When the particles aggregate as the θ_p increases, the citrate-protecting layer is less compact at the particle−particle junction. Consequently, there are vacant sites for easier CO oxidation. To examine whether the presence of a citrate layer plays a significant role in CO oxidation, an ensemble electrode with 3-nm particles ($\theta_p = \sim 2\%$) was subjected to a potential cycling treatment between −0.25 and 1.4 V in 0.1 M $HClO_4$. Above 1.0 V the adsorbed citrate is oxidized to CO_2 as demonstrated in recent in situ IR spectroscopic studies.[46,47] The anodic segments of cyclic voltammograms of CO oxidation on the electrode before and after such a treatment are nearly identical under the same experimental conditions (Figure 4),

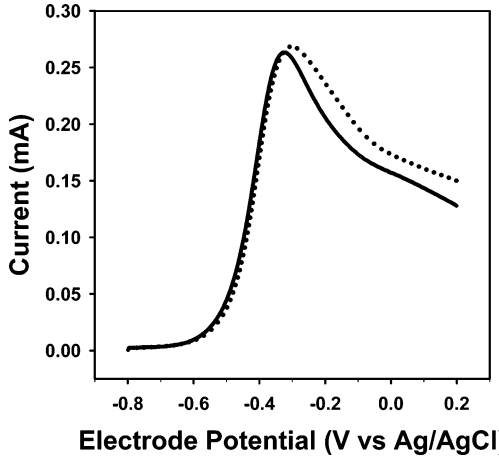

Figure 4. Anodic segments of cyclic voltammograms for CO oxidation on an ensemble electrode of 3-nm Au particles in CO-saturated 0.1 M NaOH before (dotted trace) and after (solid trace) removal of citrate layer. Particle coverage = 0.02. Scan rate = 0.1 V s^{-1}.

indicating that the citrate layer does not play a significant role in the CO oxidation on the Au nanoparticles. In contrast, if the Au particles were coated with Pt thin films, the adsorption of citrate was found to block CO and methanol oxidation. The poisoned surface can be activated by cycling to 1.0 V where citrate is oxidized on Pt.[48]

A third effect of particle aggregation is the formation of a new structure at the particle junctions. Carbon monoxide oxidation is known to be sensitive to the crystallographic orientation of the surface.[41,49] Weaver et al. systematically examined CO electrooxidation on Au single-crystal surfaces with various crystal orientations by combining cyclic voltammetry and in situ IR spectroscopy.[41,49] Electrochemical kinetic data revealed that the apparent rate constant for the (110) orientation is more than 50 times larger than that for the (111) face.[41,49] It is therefore possible that the apparent enhancement of CO oxidation activity with increasing particle coverage could also be from the formation of a more active new structure. However, this possibility is unlikely significant in the present case since the current density would then increase with increasing θ_p at a fixed potential negative to the peak value (e.g., −0.5 V). In addition, particles with drastically different sizes show similar trends in the coverage-dependent CO oxidation. Nonetheless, to disentangle the particle aggregation effect, we are using uniform particle arrays made by utilizing diblock copolymer as a template to further explore the particle coverage effect on CO oxidation and O_2 reduction. The particle size in these uniform particle arrays can be kept constant, while the interparticle distance hence the particle density can be varied systematically.[50] These systems are ideal for investigating particle size, shape, and interparticle distance effects on the reactivity. Preliminary data on CO oxidation show similar trends as observed here, which further confirm the insignificance of the structure effect arising from the particle aggregation. These results will be submitted for publication in a separate communication.

V. Conclusions

We have demonstrated that variable amounts of Au nanoparticles can be attached to ITO glass slides functionalized with APTMS, forming nanoparticle ensemble electrodes with controllable particle coverage. Electrooxidation of solution carbon monoxide was examined on these ensemble electrodes in alkaline solutions. A unique feature of this system is that the bare or APTMS-coated ITO electrodes are not active in the CO oxidation, allowing studies of the reaction on Au nanoparticles without the need to block ITO sites under suitable potential scan rates. The nanoparticle ensemble electrodes can then be treated as a system with the reaction active sites decorated in an inert matrix. The distribution of the active sites was assessed by AFM. Cyclic voltammograms showed that the apparent reactivity of particle ensemble electrode toward CO oxidation increases with nanoparticle coverage. Kinetic analysis of the voltammetric results revealed that the apparent rate constant increases with θ_p. The enhancement in the observed rate constant can be explained qualitatively in terms of the transition of the CO diffusion pattern from a more efficient mixed spherical and linear diffusion at low θ_p to a linear mass transport at higher θ_p. Although particle aggregation may complicate the explanation, the corroboration between the experimental results and the model predictions strongly suggests that the major contribution to the particle coverage effects is from the diffusion mode change. Given the increasing interest in using nanoparticle electrodes in electrocatalysis,[3] it is important to note that the shift in peak potential can come from the changes in the reactant mass transport instead of the surface reactivity.

Acknowledgment. Financial support from Miami University through start-up funds is greatly appreciated. Acknowledgment is made to the Donors of the American Chemical Society Petroleum Research Fund for partial support of this research. We thank Professor Israel Rubinstein (Weizmann Institute of Science) for providing a preprint of ref 39 and Professor James Cox (Miami University) for helpful discussion.

Supporting Information Available: Cyclic voltammograms of ensemble electrodes with 3-nm Au particles in 0.1 M NaOH used for accessing the effective Au area are provided. This material is available free of charge via the Internet at http://pubs.acs.org.

References and Notes

(1) Somorjai, G. A. *Introduction to Surface Chemistry and Catalysis*; Wiley: New York, 1994.
(2) *Electrocatalysis*; Lipkowski, J., Ross, P. N., Eds.; Wiley-VCH: New York, 1998.
(3) *Catalysis and Electrocatalysis at Nanoparticle Surfaces*; Wieckowski, A., Savinova, E. R., Vayenas, C. G., Eds.; Marcel Dekker: New York, 2003.
(4) Somorjai, G. A. *J. Phys. Chem. B* **2002**, *106*, 9201.
(5) Somorjai, G. A.; Yang, M. C. *Top. Catal.* **2003**, *24*, 61.
(6) Haruta, M. *Catal. Today* **1997**, *36*, 153.
(7) Valden, M.; Lai, X.; Goodman, D. W. *Science* **1998**, *281*, 1647.
(8) El-Deab, M. S.; Ohsaka, T. *Electrochim. Acta* **2002**, *47*, 4255.
(9) El-Deab, M. S.; Ohsaka, T. *Electrochem. Commun.* **2002**, 4z, 288.
(10) Ahmadi, T. S.; Wang, Z. L.; Green, T. C.; Henglein, A.; El-Sayed, M. A. *Science* **1996**, *272*, 1924.
(11) Ahmadi, T. S.; Wang, Z. L.; Henglein, A.; El-Sayed, M. A. *Chem. Mater.* **1996**, *8*, 1161.
(12) Sun, Y. G.; Xia, Y. N. *Science* **2002**, *298*, 2176.
(13) Sau, T. K.; Murphy, C. J. *J. Am. Chem. Soc.* **2004**, *126*, 8648.
(14) Narayanan, R.; El-Sayed, M. A. *J. Am. Chem. Soc.* **2004**, *126*, 7194.
(15) Narayanan, R.; El-Sayed, M. A. *Nano Lett* **2004**, *4*, 1343.
(16) Narayanan, R.; El-Sayed, M. A. *Langmuir* **2005**, *21*, 2027.
(17) Grunes, J.; Zhu, J.; Yang, M. C.; Somorjai, G. A. *Catal. Lett.* **2003**, *86*, 157.
(18) Jin, Y. D.; Shen, Y.; Dong, S. J. *J. Phys. Chem. B* **2004**, *108*, 8142.
(19) Luo, J.; Jones, V. W.; Maye, M. M.; Han, L.; Kariuki, N. N.; Zhong, C. J. *J. Am. Chem. Soc.* **2002**, *124*, 13988.
(20) Luo, J.; Maye, M. M.; Lou, Y. B.; Han, L.; Hepel, M.; Zhong, C. J. *Catal. Today* **2002**, *77*, 127.
(21) Maye, M. M.; Luo, J.; Han, L.; Kariuki, N. N.; Zhong, C. J. *Gold Bull.* **2003**, *36*, 75.
(22) Cuenya, B. R.; Baeck, S. H.; Jaramillo, T. F.; McFarland, E. W. *J. Am. Chem. Soc.* **2003**, *125*, 12928.

(23) Jaramillo, T. F.; Baeck, S. H.; Cuenya, B. R.; McFarland, E. W. *J. Am. Chem. Soc.* **2003**, *125*, 7148.

(24) Friedrich, K. A.; Henglein, F.; Stimming, U.; Unkauf, W. *Electrochim. Acta* **2000**, *45*, 3283.

(25) Maillard, F.; Eikerling, M.; Cherstiouk, O. V.; Schreier, S.; Savinova, E.; Stimming, U. *Faraday Discuss.* **2004**, *125*, 357.

(26) Maillard, F.; Savinova, E. R.; Simonov, P. A.; Zaikovskii, V. I.; Stimming, U. *J. Phys. Chem. B* **2004**, *108*, 17893.

(27) Maillard, F.; Schreier, S.; Hanzlik, M.; Savinova, E. R.; Weinkauf, S.; Stimming, U. *Phys. Chem. Chem. Phys.* **2005**, *7*, 385.

(28) Gueshi, T.; Tokuda, K.; Matsuda, H. *J. Electroanal. Chem.* **1979**, *101*, 29.

(29) Amatore, C.; Saveant, J. M.; Tessier, D. *J. Electroanal. Chem.* **1983**, *147*, 39.

(30) Scharifker, B. R. *J. Electroanal. Chem.* **1988**, *240*, 61.

(31) Lee, H. J.; Beriet, C.; Ferrigno, R.; Girault, H. H. *J. Electroanal. Chem.* **2001**, *502*, 138.

(32) Finklea, H. O.; Snider, D. A.; Fedyk, J.; Sabatani, E.; Gafni, Y.; Rubinstein, I. *Langmuir* **1993**, *9*, 3660.

(33) Finklea, H. O.; Snider, D. A.; Fedyk, J. *Langmuir* **1990**, *6*, 371.

(34) Brown, K. R.; Walter, D. G.; Natan, M. J. *Chem. Mater.* **2000**, *12*, 306.

(35) Grabar, K. C.; Freeman, R. G.; Hommer, M. B.; Natan, M. J. *Anal. Chem.* **1995**, *67*, 735.

(36) Freeman, R. G.; Grabar, K. C.; Allison, K. J.; Bright, R. M.; Davis, J. A.; Guthrie, A. P.; Hommer, M. B.; Jackson, M. A.; Smith, P. C.; Walter, D. G.; Natan, M. J. *Science* **1995**, *267*, 1629.

(37) Cheng, W. L.; Dong, S. J.; Wang, E. K. *Chem. Mater.* **2003**, *15*, 2495.

(38) Ron, H.; Rubinstein, I. *Langmuir* **1994**, *10*, 4566.

(39) Wanunu, M.; Popovitz-Biro, R.; Cohen, H.; Vaskevich, A.; Rubinstein, I. *J. Am. Chem. Soc.* **2005**, *127*, 9207.

(40) Ca, D. A.; Cox, J. A. *Electrochim. Acta*, in press.

(41) Chang, S. C.; Hamelin, A.; Weaver, M. J. *J. Phys. Chem.* **1991**, *95*, 5560.

(42) Roberts, J. L.; Sawyer, D. T. *Electrochim. Acta* **1965**, *10*, 989.

(43) Bard, A. J.; Faulkner, L. R. *Electrochemical Methods*, 2nd ed.; John Wiley & Sons: New York, 2001; p 235.

(44) Although the model is for reversible reactions, qualitatively the conclusions are also applicable to irreversible reactions.

(45) Baker, W. S.; Crooks, R. M. *J. Phys. Chem. B* **1998**, *102*, 10041.

(46) Nichols, R. J.; Burgess, I.; Young, K. L.; Zamlynny, V.; Lipkowski, J. *J. Electroanal. Chem.* **2004**, *563*, 33.

(47) Floate, S.; Hosseini, M.; Arshadi, M. R.; Ritson, D.; Young, K. L.; Nichols, R. J. *J. Electroanal. Chem.* **2003**, *542*, 67.

(48) Kumar, S.; Zou, S. In preparation.

(49) Edens, G. J.; Hamelin, A.; Weaver, M. J. *J. Phys. Chem.* **1996**, *100*, 2322.

(50) Spatz, J. P.; Mossmer, S.; Hartmann, C.; Moller, M.; Herzog, T.; Krieger, M.; Boyen, H. G.; Ziemann, P.; Kabius, B. *Langmuir* **2000**, *16*, 407.